XVI International Conference on Durability of Building Materials and Components
DBMC 2023, China
K.F. Li and D.P. Fang (Eds)

Chemo-physical Analysis on Corrosion Initiation of Offshore Structures under Chloride Attack

Bin Dong[1], Yuguo Yu[2] and Wei Gao[1]

[1]Centre for Infrastructure Engineering and Safety, School of Civil and Environmental Engineering, The University of New South Wales, Sydney, NSW 2052, Australia, bin.dong2@unsw.edu.au(Bin Dong), w.gao@unsw.edu.au(Wei Gao)

[2]Research Center for Wind Engineering and Engineering Vibration, Guangzhou University, Guangzhou 510006, China, yuguo.yu@gzhu.edu.cn(Yuguo Yu)

Abstract. *Chloride ingress has been recognized as a main factor inducing the corrosion of offshore reinforced concrete structures. It is acknowledged that the chemical attack can lead to concrete property deterioration, which inevitably affects the reinforcement corrosion. Herein, the influence of the concrete aging on the chloride-induced corrosion initiation is systematically evaluated by a novel numerical framework. In this framework, the chemo-physical analysis is conducted based on coupled Nernst-Planck model and Gibbs energy minimization model. The proposed method is first validated against reported experimental results. It is found that the chloride ingress is always accompanied by leaching of hydrates near the exposure surface, leading to the porosity enlargement. Moreover, due to chemical binding of chloride to monosulfoaluminate, ettringite continuously precipitates under the function of released sulfate ions. Through a series of numerical analyses, it is revealed that the newly formed hydrates impose competitive effects on chloride transportation due to the simultaneous pore-clogging and expansion-induced microcracks. Chloride-induced corrosion occurs earlier in the situation that the effect of microcracks overcomes that of pore clogging, otherwise, the corrosion is delayed.*

Keywords: *Chemo-physical Analysis, Chloride Ingress, Corrosion Initiation, Concrete Aging, Reinforced Concrete.*

1 Introduction

Chloride-induced corrosion of reinforcements has been recognized as one serious long-term durability concern for offshore reinforced concrete structures (Yu et al., 2019). The corrosion process during the structural service life is generally divided into two stages (Xia et al., 2019), namely corrosion initiation and propagation, see Figure 1. During the initiation phase, chloride from the harsh marine environment penetrates concrete and destroys the passive film on the steel surface. Once the steel is depassivated to some extent, the corrosion accelerates remarkably and enters the propagation stage. As the corrosion further proceeds, corrosion products accumulate on the concrete-steel interface, leading to the cracking and spalling of the cover concrete. To ensure structural safety, precise estimation of the chloride-induced corrosion initiation is essential.

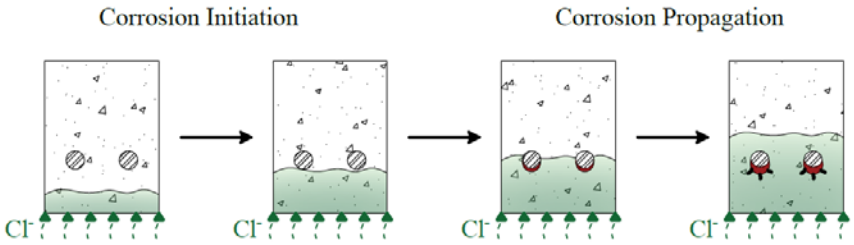

Figure 1. Chloride-induced corrosion process of reinforced concrete

To achieve this goal, an index called critical chloride content has been proposed by researchers (Angst et al., 2009). In this way, the corrosion initiation can be determined by evaluating the chloride content on the steel surface, where various numerical studies have been reported for modelling the chloride distribution (Cheng et al., 2018; Dong et al., 2023; Xia et al., 2019; Zhang et al., 2020). Fick's second law is applied to the chloride transportation analysis in some studies (Cheng et al., 2018; Zhang et al., 2020), which, however, is oversimplified to neglect the coupling between chloride and other ions. To deal with this problem, the tendency of applying well-known Planck-Nernst model to assess the multi-ionic transportation process gradually enhances (Dong et al., 2023; Xia et al., 2019). Nevertheless, most of these modelling techniques do not take the interaction between ionic species and hydrates into account. It has been reported that during the chloride ingress process, the leaching of hydrates also happens near the exposure surface (Cherif et al., 2020), which causes the increase of porosity. On the other hand, the chloride can potentially exchange the sulfate ion in monosulfoaluminate (AFm), i.e., chemical binding (Yu et al., 2019; Yu et al., 2022; Yu et al., 2020; Yu et al., 2021). This phenomenon can lead to the formation of hydrates, such as Friedel salt and ettringite (AFt), which possibly clog pores of concrete. Evidently, the property deterioration of concrete, i.e., concrete aging, could significantly influence the chloride ingress, and ignoring this factor could cause the misestimation of the corrosion initiation.

To fill this research gap, a novel chemo-physical modelling framework is proposed in this paper for analyzing the concrete aging-affected corrosion initiation. The Planck-Nernst model is applied to evaluate the multi-ionic transportation, while the Gibbs energy minimization method is employed for thermodynamic analysis of the time-variant chemical system. Detailed description of the modelling framework is presented in Section 2. Following validation against experimental study in Section 3, a series of numerical studies are conducted to systematically evaluate the influence of concrete aging on corrosion initiation in Section 4. Some concluding remarks are presented in Section 5.

2 Model Formulation

This chemo-physical modelling framework is based on the operator splitting approach (Yu et al., 2019; Yu et al., 2022; Yu et al., 2020; Yu et al., 2021), where the reactive transportation problem is decoupled to be the sequentially solved multi-ionic transportation analysis and chemical reaction analysis. The validity and efficiency of this method has been evaluated and proved in previous studies (Yu et al., 2019; Yu et al., 2022; Yu et al., 2020; Yu et al., 2021). In

this study, the Nernst-Planck model under the electroneutrality condition is employed to analyze multi-ionic transportation (Dong et al., 2023).

$$w_{\mathrm{L}}\frac{\partial c_i}{\partial t}-\nabla\cdot\left(\underbrace{D_i w_{\mathrm{L}}\nabla c_i}_{\text{diffusion}}+\underbrace{\frac{D_i z_i \mathrm{F}}{\mathrm{R}T}c_i w_{\mathrm{L}}\nabla\varphi}_{\text{electro-migration}}+\underbrace{D_i w_{\mathrm{L}} c_i\nabla\ln\gamma_i}_{\text{chemical activity coupling}}\right)=0 \tag{1}$$

$$-\nabla\cdot\left[\mathrm{F}w_{\mathrm{L}}\sum D_i z_i\nabla c_i+\frac{\mathrm{F}^2 w_{\mathrm{L}}}{\mathrm{R}T}\sum D_i z_i^2 c_i\nabla\varphi+\mathrm{F}w_{\mathrm{L}}\sum D_i z_i c_i\nabla\ln\gamma_i\right]=0 \tag{2}$$

where c_i, $\boldsymbol{Q}_i$, D_i, γ_i are the concentration, flux, diffusion coefficient and chemical activity coefficient of the ith ion, respectively, w_{L} is volume fraction of liquid water in the porous material, F is the Faraday constant, R is the ideal gas, T is the thermodynamic temperature of concrete, φ is the electric potential in concrete.

The transportation of the ionic species alters the chemical environment in the concrete, leading to complex chemical reactions, such as leaching and chloride binding. Herein, these chemical reactions are evaluated by thermodynamic modelling method, where Gibbs energy minimization method (GEM) is adopted (Kulik et al., 2013).

$$\min_{\boldsymbol{n}} G=\boldsymbol{n}^{\mathrm{T}}\boldsymbol{\mu}\quad\text{subject to}\begin{cases}\mathbf{W}\boldsymbol{n}=\boldsymbol{b}\\ \mathbf{C}\boldsymbol{n}=\mathbf{0}\\ \boldsymbol{n}\geq\mathbf{0}\end{cases} \tag{3}$$

where G is the total Gibbs energy of the chemical system, $\boldsymbol{n}$ is the molar composition vector of the chemical system, $\boldsymbol{\mu}$ is the chemical potential of species, $\mathbf{W}$ is the formula matrix of species, $\boldsymbol{b}$ is the molar abundance vector of the chemical elements and $\mathbf{C}$ is the vector of electrical charges of species.

The dissolution and precipitation of hydrates could lead to the change of concrete porosity and ionic diffusivity, which is calculated as:

$$f(\theta)=\left(\frac{\theta(t)}{\theta_0}\right)^3\left(\frac{1-\theta_0}{1-\theta(t)}\right)^2;\quad\theta(t)=\theta_0-\sum_j\widetilde{V}_j\left(n_j(t)-n_{j0}\right) \tag{4}$$

where $f(\theta)$ denotes the effect of the porosity change on the ionic diffusion coefficient, θ_0 and $\theta(t)$ are the initial porosity and porosity at time t, n_{j0} and $n_j(t)$ means the initial amount and amount of substances at time t of jth hydrate, $\widetilde{V}_j$ is molar volume of jth hydrate.

On the other hand, AFt may form during the chloride ingress process due to the chemical binding of chloride. It has been widely accepted that the newly precipitated AFt could exert pressure on the shrinking pore space (Yu et al., 2015), which could generate microcracks and

facilitate the diffusivity of ions. In this model, this factor is considered by an empirical model (Sarkar et al., 2010).

$$\overline{\Delta V_{\mathrm{E}}} = \Delta V_{\mathrm{S}}^{\mathrm{AFt}} - b\theta\overline{V};\ \Delta V_{\mathrm{S}}^{\mathrm{AFt}} = {}^{f}V_{\mathrm{S}}^{\mathrm{AFt}} - {}^{i}V_{\mathrm{S}}^{\mathrm{AFt}} \tag{5}$$

$$\bar{\varepsilon} = \frac{\overline{\Delta V_{\mathrm{E}}}}{\overline{\overline{\Delta V}}};\ \ \bar{\bar{\varepsilon}} = \frac{\bar{\varepsilon}}{3};\ \ \text{for } \overline{\Delta V_{\mathrm{E}}} > 0 \tag{6}$$

$$C_{\mathrm{d}} = k(1 - \frac{\varepsilon^{\mathrm{th}}}{\bar{\bar{\varepsilon}}})^{m};\ \ \text{for } \bar{\bar{\varepsilon}} > \varepsilon^{\mathrm{th}} \tag{7}$$

$$f(C_{\mathrm{d}}) = (1 + \frac{32}{9}C_{\mathrm{d}}) + D_{\mathrm{P}} \tag{8}$$

$$D_{\mathrm{P}} = \begin{cases} 0; & C_{\mathrm{d}} \le C_{\mathrm{dc}} \\ \dfrac{(C_{\mathrm{d}} - C_{\mathrm{dc}})^2}{(C_{\mathrm{dec}} - C_{\mathrm{d}})}; & C_{\mathrm{dc}} < C_{\mathrm{d}} < C_{\mathrm{dec}} \\ (C_{\mathrm{dec}} - C_{\mathrm{dc}})^2; & C_{\mathrm{d}} \ge C_{\mathrm{dec}} \end{cases} \tag{9}$$

where $\overline{V}$ indicates representative element volume, $\Delta V_{\mathrm{S}}^{\mathrm{AFt}}$ is volumetric growth of AFt phase, ${}^{i}V_{\mathrm{S}}^{\mathrm{AFt}}$ is the initial volume of AFt phase without disturbance of system equilibrium, ${}^{f}V_{\mathrm{S}}^{\mathrm{AFt}}$ is the volume of AFt phase after chloride ingress, where fresh AFt may precipitate, $\overline{\Delta V_{\mathrm{E}}}$ and $\bar{\varepsilon}$ are volumetric expansion and strain, $\bar{\bar{\varepsilon}}$ is uniaxial strain, $\varepsilon^{\mathrm{th}}$ is threshold strain at which crack emerges, C_{d} is crack density, b, k and m are empirical parameters, where 0.5, 2.3 and 2×10^{-4} are assigned to k, m and $\varepsilon^{\mathrm{th}}$ respectively. Note that b indicates capability of the pore space to freely accommodate the AFt without being stressed, and the value of the parameter ranges from 0.05 to 0.45 (Yu et al., 2021). $f(C_{\mathrm{d}})$ shows effect of microcracks on ionic diffusivity, $C_{\mathrm{dc}} = 0.18$ and $C_{\mathrm{dec}} = 0.56$ are empirical percolation thresholds.

3 Model Validation

The effectiveness of the proposed modelling approach is examined herein by studying a long-term chloride ingress experiment (Li et al., 2021). The schematic diagram of the experimental work is illustrated in Figure 2, and detailed material properties, such as ionic concentration, hydrates content and microstructure, are referred to the reported study (Li et al., 2021). Based on Cemdata18 (Lothenbach et al., 2019), a famous database for cementitious material, the simulated and experimental chloride distribution are compared in Figure 3.

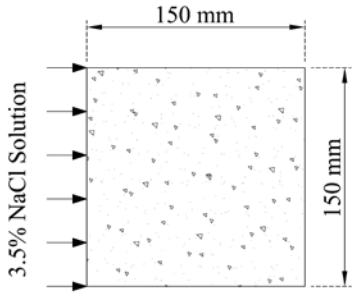

Figure 2. Schematic diagram of experimental setting for chloride ingress

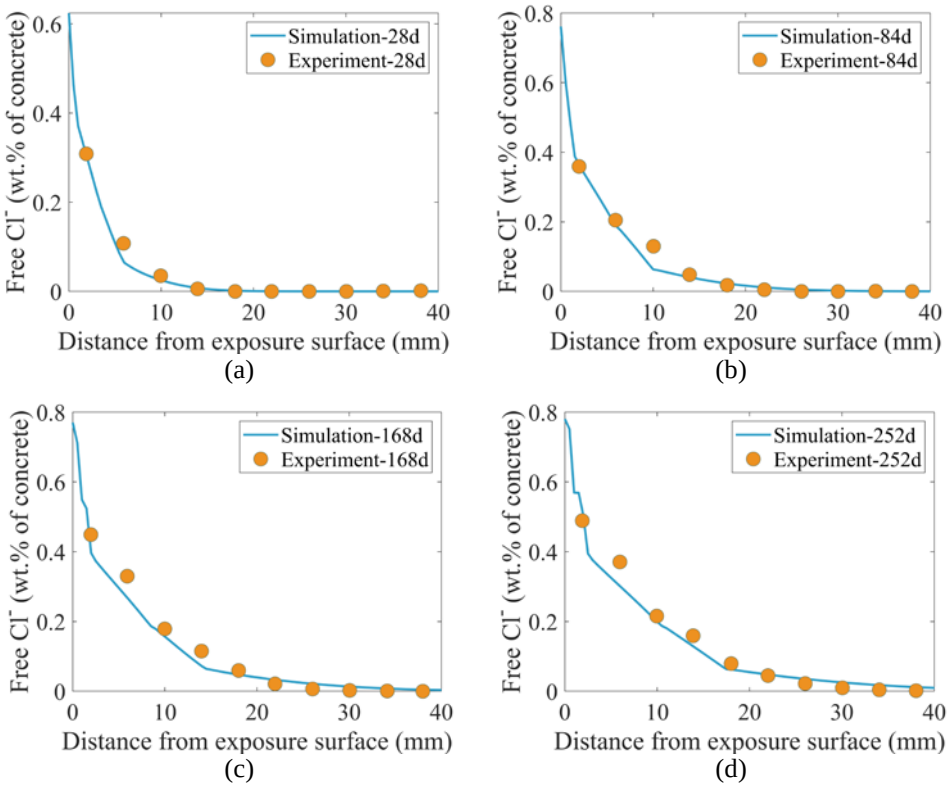

Figure 3. Simulated and experimental chloride distribution: (a) day 28; (b) day 84; (c) day 168; (d) day 252

As shown in Figure 3, the simulated and experimental results agree perfectly throughout the exposure period, which demonstrates the validity of the proposed framework. Moreover, it is evident that the surface chloride content increases with the continuous chloride ingress. To explain this interesting finding, the hydrates composition and corresponding porosity are assessed and shown in Figure 4.

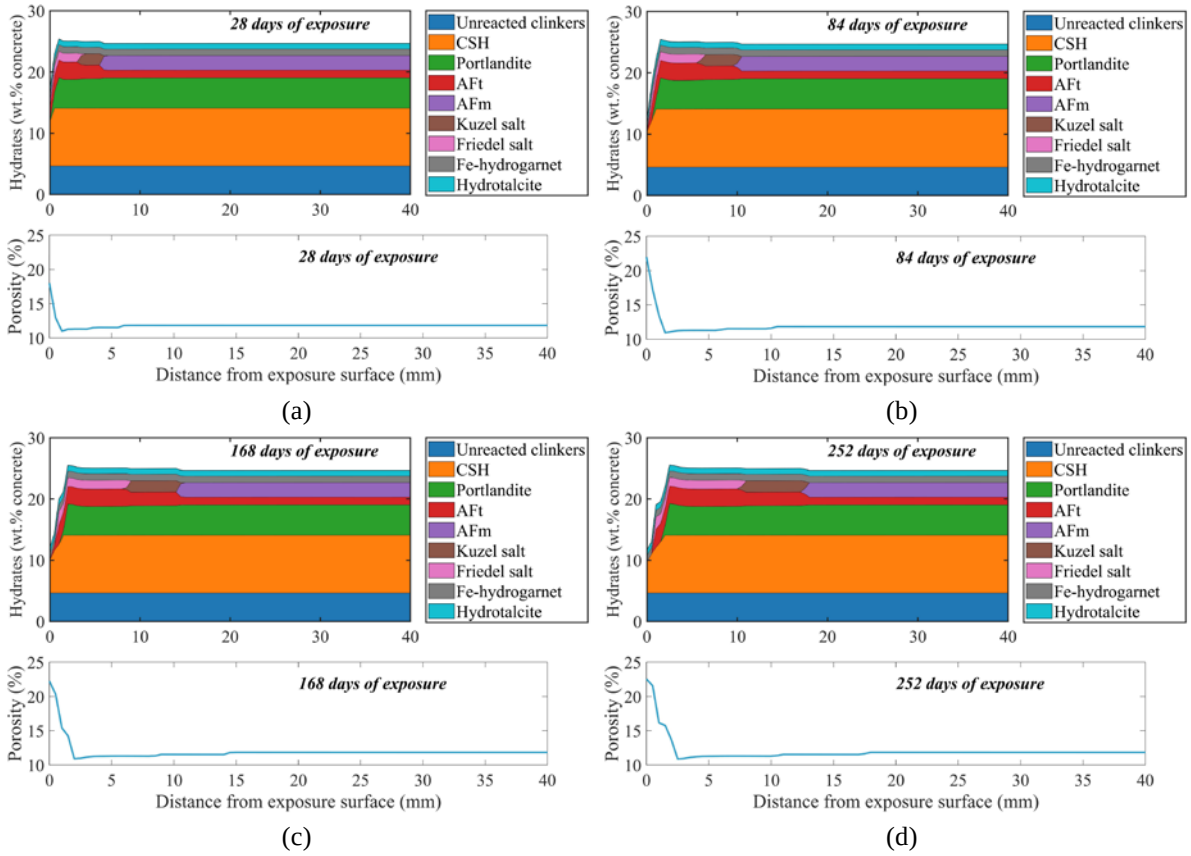

Figure 4. Hydrates composition and porosity of aged concrete: (a) day 28; (b) day 84; (c) day 168; (d) day 252

The leaching of hydrates and corresponding porosity enlargement near the exposure surface are illustrated in Figure 4, which explains the continuous increase of surface chloride content. Moreover, it is also showcased that the Kuzel salt is formed before the Friedel salt during the binding process of chloride, which is consistent with previous study (Guo et al., 2022). Except these direct products of the chemical binding, the sulfate released by the consumed AFm facilitates the formation of AFt, see Figure 4. Indeed, the porosity decreases due to these newly precipitated hydrates, which was also discovered in the experimental study (Cherif et al., 2020).

4 Numerical Analyses and Discussions

Following the validation, the model is further employed to evaluate the effect of concrete aging on corrosion initiation by an illustrative example, as illustrated in Figure 5. In previous study, it was found that the effect of the newly formed AFt on the chloride ingress highly depends on the availability of free pore space to accommodate the substance (Yu et al., 2021). Therefore, different values of b are considered in numerical analyses, which are 0.05, 0.1,0.15 and 0.2. respectively. Moreover, in the following discussions, corrosion initiation is indicated by the fact that the chloride content on steel surface reaches the critical chloride content, which is assumed as 0.08% by weight of binder (Xia et al., 2019). The corrosion initiation time is listed in Table 1, where the aging effect is not considered in the control model with constant $f(\theta)$ equal to 1.

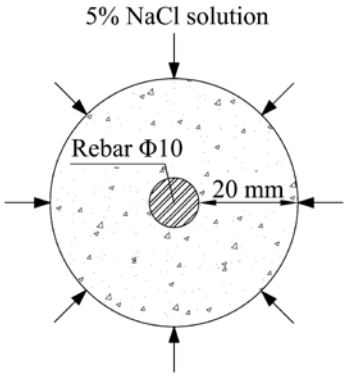

Figure 5. Schematic diagram of numerical example

Table 1. Corrosion initiation in different conditions

Model setting	*Corrosion initiation (days)*
control	75.25
$b = 0.05$	50.08
$b = 0.1$	64.91
$b = 0.15$	77.25
$b = 0.2$	77.25

According to Table 1, it is found that the concrete aging advances corrosion initiation once the pore space to permit free expansion of hydrates is limited. However, with enough available pore space, the corrosion initiation is delayed under the effect of concrete aging. This interesting phenomenon could be explained by the competitive effects caused by the newly formed AFt. As illustrated in Figure 6, the pore-clogging induced by the AFt may decelerate the penetration of chloride. On the other hand, Figure 6 also shows that chloride ingress may be accelerated due to more transportation paths provided by AFt-induced microcracks. With decreasing b, the effect of microcrack gradually overcomes that of pore-clogging, leading to early corrosion initiation.

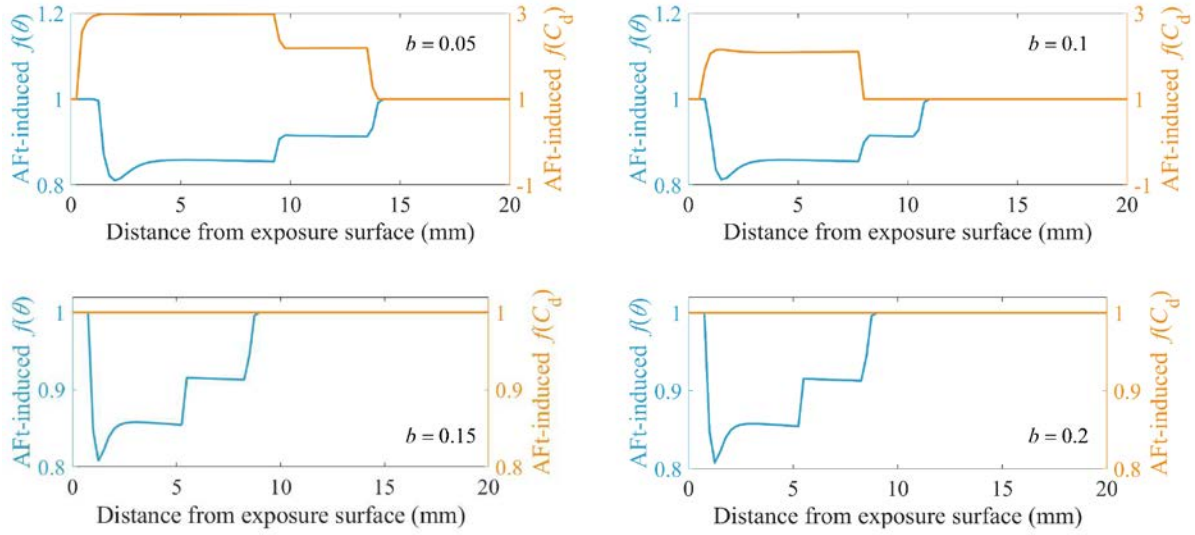

Figure 6. Competitive effects of microcracks and pore-clogging induced by newly formed AFt at day 50

5 Conclusions

The proposed chemo-physical modelling framework is demonstrated to be an effective approach to estimate the concrete aging-affected corrosion initiation of reinforcements. Benefitting from this modelling technique, the influence of concrete aging on chloride-induced corrosion initiation is discovered to be dependent on competitive effects of newly formed AFt during chloride ingress. Concrete aging facilitates the corrosion initiation in the situation that the effect of AFt-induced microcracks overcomes that of pore clogging, otherwise, the aging delayed the occurrence of corrosion.

Acknowledgements

The research work presented in this paper has been supported by Australian Research Council project IH200100010, DP210101353 and IH210100048. The presented numerical computations are undertaken with the assistance of resources and services from the National Computational Infrastructure (NCI), which is supported by the Australian Government.

References

Angst, U., Elsener, B., Larsen, C. K. and Vennesland, Ø. (2009). *Critical chloride content in reinforced concrete—A review*, Cement and Concrete Research, 39(12), 1122-1138.

Cheng, X., Su, Q., Ma, F., Liu, X. and Liang, X. (2018). *Investigation on crack propagation of concrete cover induced by non-uniform corrosion of multiple rebars*, Engineering Fracture Mechanics, 201, 366-384.

Cherif, R., Hamami, A. E. A. and Ait-Mokhtar, A. (2020). *Effects of leaching and chloride migration on the microstructure and pore solution of blended cement pastes during a migration test*, Construction and Building Materials, 240, 117934.

Dong, B., Yu, Y., Gao, W. and Zhao, G. (2023). *A novel method for chloride-induced corrosion analysis incorporating consistent ionic diffusivity and concrete resistivity*, Construction and Building Materials, 365, 129941.

Guo, B., Qiao, G., Han, P., Li, Z. and Fu, Q. (2022). *Effect of natural carbonation on chloride binding behaviours in OPC paste investigated by a thermodynamic model*, Journal of Building Engineering, 49, 104021.

Kulik, D. A., Wagner, T., Dmytrieva, S. V., Kosakowski, G., Hingerl, F. F., Chudnenko, K. V. and Berner, U. R. (2013). *GEM-Selektor geochemical modeling package: revised algorithm and GEMS3K numerical kernel for coupled simulation codes*, Computational Geosciences, 17, 1-24.

Li, C.-z., Song, X.-b. and Jiang, L. (2021). *A time-dependent chloride diffusion model for predicting initial corrosion time of reinforced concrete with slag addition*, Cement and Concrete Research, 145, 106455.

Lothenbach, B., Kulik, D. A., Matschei, T., Balonis, M., Baquerizo, L., Dilnesa, B., Myers, R. J. (2019). *Cemdata18: A chemical thermodynamic database for hydrated Portland cements and alkali-activated materials*, Cement and Concrete Research, 115, 472-506.

Sarkar, S., Mahadevan, S., Meeussen, J. C. L., Van der Sloot, H. and Kosson, D. S. (2010). *Numerical simulation of cementitious materials degradation under external sulfate attack*, Cement and Concrete Composites, 32(3), 241-252.

Xia, J., Li, T., Fang, J. X. and Jin, W. l. (2019). *Numerical simulation of steel corrosion in chloride contaminated concrete*, Construction and Building Materials, 228, 116745-116745.

Yu, Y., Chen, X., Gao, W., Wu, D. and Castel, A. (2019). *Impact of atmospheric marine environment on cementitious materials*, Corrosion Science, 148, 366-378.

Yu, Y., Dong, B., Gao, W. and Sofi, A. (2022). *Physics-based stochastic aging corrosion analysis assisted by machine learning*, Probabilistic Engineering Mechanics, 69, 103270.

Yu, Y., Gao, W., Castel, A., Liu, A., Feng, Y., Chen, X. and Mukherjee, A. (2020). *Modelling steel corrosion under concrete non-uniformity and structural defects*, Cement and Concrete Research, 135, 106109-106109.

Yu, Y., Gao, W., Feng, Y., Castel, A., Chen, X. and Liu, A. (2021). *On the competitive antagonism effect in combined chloride-sulfate attack: A numerical exploration*, Cement and Concrete Research, 144, 106406-106406.

Yu, Y., Zhang, Y. X. and Khennane, A. (2015). *Numerical modelling of degradation of cement-based materials under leaching and external sulfate attack*, Computers & Structures, 158, 1-14.

Zhang, G., Tian, Y., Jin, X., Zeng, Q., Jin, N., Yan, D. and Tian, Z. (2020). *A self-balanced electrochemical model for corrosion of reinforcing steel bar in considering the micro-environments in concrete*, Construction and Building Materials, 254, 119116-119116.